17

Behavior of Aging, Micro-Void, and Self-Healing of Glass/Ceramic Materials and Its Effect on Mechanical Properties

Wenning Liu, Xin Sun and Moe Khaleel
Pacific Northwest National Laboratory, Richland
USA

1. Introduction

Among the high-efficiency energy conversion devices that are environmentally friendly with little or no toxic emissions, the solid oxide fuel cell (SOFC) continues to show great promise as a future power source. It has potential applications in stationary power generation and as auxiliary power units. Among various SOFC designs under development, anode-supported planar cells have shown great potential in delivering high performance at reasonable costs (Teagan et al., 2000; Chung et al. 2005). Planar SOFCs offer a significant advantage of a compact design along with higher power densities. In the meantime, they require that hermetic gas seals be incorporated for efficient and effective channeling of fuel and oxygen.

Seals are the most critical components in commercializing the planar SOFC technology (Nielsen et al., 2007; Choi & Bansal, 2005; Smeacetto et al., 2008). They must adequately prevent air and fuel from leaking, effectively isolate the fuel from the oxidant, and insulate the cell from short circuit. Essentially, there are two standard methods for sealing: compressive sealing and rigid bonding (Singh, 2007; Fergus, 2005; Chou et al., 2003). In compressive sealing, a compliant, high-temperature material is captured between the two sealing surfaces and compressed with a load frame external to the stack to deliver hermetic sealing. The sealing surfaces can slide with respect to one another without disrupting the hermeticity of the seal. This technology, however, remains incomplete due to the lack of a reliable, high-temperature, sealing material (Simner & Stevenson, 2001) and the difficulty of designing the appropriate load frame under high-operating temperatures. Rigid seals rely on effective bonding of the seal material to the sealing surfaces. They offer significant advantages over compressive seals that suffer from problems of oxide scaling and chemical stability under highly reactive environments in addition to the disadvantages of incorporating an externally applied load (Singh, 2007).

As a rigid seal, glass joining provides a cost-effective and relatively simple method for bonding ceramic and metal parts. However, the softening point of the glass component typically limits the maximum operating temperature to which the joint may be exposed. As discussed by Weil et al. (2004), there are a number of other key materials and processing variables that can influence the performance of glass seals, including the composition of the metal substrate against which the seal is made, the operating parameters, such as the

expected lifetime of the device (and therefore the seals), and the degree of thermal cycling to which the seals will be exposed during system operation. In addition, a glass seal in room temperature is brittle, non-yielding, and particularly susceptible to fracture when exposed to tensile stresses. Because of these complications, much of the development effort for SOFC seal materials has been focused on developing materials that have compatible, temperature-dependent, coefficients of thermal expansion (CTEs) for each of the components being jointed, i.e., the ceramic cell, the seal, and the metal separator, to minimize the buildup of residual stresses within the joint. Only a handful of high-temperature glass compositions in the borate- or phosphate-doped aluminosilicate families satisfy these requirements (Lahl et al., 1999). The glass seal composition used in this study, designated as G18 (Meinhardt et al., 2002), was developed by Pacific Northwest National Laboratory (PNNL) for planar-type SOFC applications. G18 is a barium–calcium–aluminosilicate (BCAS)-based glass with boron oxide added. Silicon-based glasses provide a better combination of chemical compatibility and stability properties than phosphate- or borate-based glasses, although this material is susceptible to chromium migration when used with ferritic stainless steels (Yang et al., 2003; Yang et al. 2004). For rigid bonds as such, stress levels in the glass seal and its mechanical properties, such as Young's modulus and interfacial strength between different interfaces, become critical for long-term reliability of the seal and therefore the stacks.

To obtain a reliable SOFC design in the complex operating environments, the stress level in the glass seal materials as well as at the various interfaces must be carefully examined and managed. To accurately predict these stresses, accurate material models that consider the various aspects of the seal materials under different operating conditions, including aging and cooling, become critical for long-term performance of the sealing system and SOFC stacks.

This chapter first describes tests to investigate the temporal evolution of the volume fraction of ceramic phases, the evolution of micro-damage, and the self-healing behavior of the glass ceramic sealant used in SOFCs Then a phenomenological model based on mechanical analogs is developed to describe the temperature-dependent Young's modulus of glass ceramic seal materials. It was found that after the initial sintering process, further crystallization of the glass ceramic sealant does not stop, but slows down and reduces the residual glass content while boosting the ceramic crystalline content. Under a long-term operating environment, distinct fibrous and needle-like crystals in the amorphous phase disappeared, and smeared/diffused phase boundaries between the glass phase and ceramic phase were observed. Meanwhile, the micro-damage was induced by the cooling-down process from the operating temperature to the room temperature, which can potentially degrade the mechanical properties of the glass/ceramic sealant. The glass/ceramic sealant self-healed upon reheating to the SOFC operating temperature, which can restore the mechanical performance of the glass/ceramic sealant. The phenomenological model developed here includes the effects of continuing aging and devitrification on the ceramic phase volume fraction, and the resulting mechanical properties of glass ceramic seal material are considered. The effects of micro-voids and self-healing are also considered using a continuum damage mechanics (CDM) model. This formulation is for glass/ceramic seals in general, and it can be further developed to account for effects of various processing parameters. This model was applied to G18, and the temperature-dependent experimental measurements were used to calibrate the modeling parameters and to validate the model prediction.

2. Material and experimental

In planar-type SOFCs, different components need to be hermetically sealed to make certain that the SOFC system functions properly. The seals prevent mixing of the fuel and oxidant and also keep the fuel from leaking out of the stack. Thus, seal integrity is essential to stack performance and operation. The glass ceramic sealant material, named G18, which was developed at PNNL, was a BCAS-based glass designed in-house. It was originally melted from the following mixture of oxides (by weight percent): 56.4% BaO, 22.1% SiO_2, 5.4% Al_2O_3, 8.8% CaO, and 7.3% B_2O_3 (Meinhardt et al., 2002). The G-18 powder was milled to an average particle size of 20 μm and mixed with a proprietary binder system to form a paste that could be dispensed onto the substrate surfaces at a uniform rate of 0.075 g/linear cm with an automated syringe dispenser. The glass paste may be dispensed onto the YSZ side of the bilayer discs of the Ni-YSZ anode and the YSZ electrolyte, which are 25 mm in diameter. Each disk was then concentrically positioned on a washer specimen, loaded with a 100-g weight, and heated in air under the following sealing schedule: heat from room temperature to 850°C at 10°C/min, hold at 850°C for 1 hour, cool to 750°C at 5°C/min, hold at 750°C for 4 hours, and cool to room temperature at 5°C/min (Weil et al., 2004).
The hermetic seal is easily formed by dispensing a paste or tape casting followed by heating. The glass wets the surfaces to be bonded at the joining temperature, and partial crystallization then provides mechanical stiffness and strength at operating temperatures.

2.1 Temporal evolution of volume fraction of ceramic (crystalline) phase

The volume fraction of the ceramic (crystalline) phase varies with aging or operating time under SOFC operating temperatures. To evaluate the temporal evolution of the ceramic phase, the phase structure of the glass-ceramic sealant was determined by X-ray diffraction (XRD). XRD finds the geometry or shape of a molecule using X-rays, based on the elastic scattering of X-rays from structures that have a long-range order. XRD relies on the dual wave/particle nature of X-rays to obtain information about the structure of crystalline materials. The dominant effect that occurs when an incident beam of monochromatic X-rays interacts with a target material is scattering of those X-rays from atoms within the target material. In materials with a regular structure (i.e., crystalline), the scattered X-rays undergo constructive and destructive interference. This is the process of diffraction. The diffraction of X-rays by crystals is described by Bragg's Law as

$$n\lambda = 2d \sin\theta \quad (1)$$

The directions of possible diffractions depend on the size and shape of the unit cell of the material. The most comprehensive description of scattering from crystals is given by the dynamical theory of diffraction (Azároff et al., 1974).
Specimens used for the XRD test were prepared according the aforementioned procedure with dimensions of 3 mm × 4 mm × 45 mm. They were heated in air under the following sealing schedule: heat from room temperature to 850°C at 10°C/min, hold at 850°C for 1 hour, cool to 750°C at 5°C/min, hold at 750°C for 4 hours, and cool to room temperature at 5°C/min. The specimen's surfaces were ground to a 600-grit finish and then ultrasonically cleaned with distilled water and acetone.
Figure 1 shows the evolution of the volume fraction of crystalline phases that form within the devitrifying glass as a function of time held at 750°C (Weil et al., 2004). This graph was

constructed from a series of quantitative XRD measurements conducted on the aged glass-ceramic samples. For glass/ceramic sealing materials, the volume fraction of the ceramic crystalline is time dependent under the SOFC operating temperature. Some volume of the ceramic crystalline is formed at the end of the initial sealing process at 850°C. The crystallization process slows down but does not stop when it is subjected to the typical operating environment of 750°C. The volume fraction of the ceramic crystalline in the sealant material is increased with the holding time in the air at the operating temperature.

After 1 hour of the initial sealing process at 850°C, the crystalline contents of $BaSiO_3$, $(Ba_{1.5}Ca_{0.5})SiO_4$, and Hexa-$BaAi_2Si_2O_8$ were observed in the glass/ceramic seal. $BaSiO_3$ is the main crystalline phase composition, taking up approximately 40% of the volume fraction. After the first 20 hours under the SOFC working temperature of 750°C, the volume fractions of both $BaSiO_3$ and $(Ba_{1.5}Ca_{0.5})SiO_4$ remained relatively unchanged, and the volume fraction of hexa-$BaAi_2Si_2O_8$ doubled from 7% to 15%. With a longer working time, the content of $(Ba_{1.5}Ca_{0.5})SiO_4$ and the hexa-$BaAi_2Si_2O_8$ began to decrease, and the content of $BaSiO_3$ started to increase. A new phase of mono-$BaAi_2Si_2O_8$ started to appear at about 150 hours of working time and continued to increase because $(Ba_{1.5}Ca_{0.5})SiO_4$ and Hexa- $BaAi_2Si_2O_8$ were both transformed into this phase. The overall crystalline phase increased almost linearly with log(time[h]) in the first 300 hours of aging. After that, the crystallization process gradually stopped, and the crystalline content in the material remained relatively unchanged.

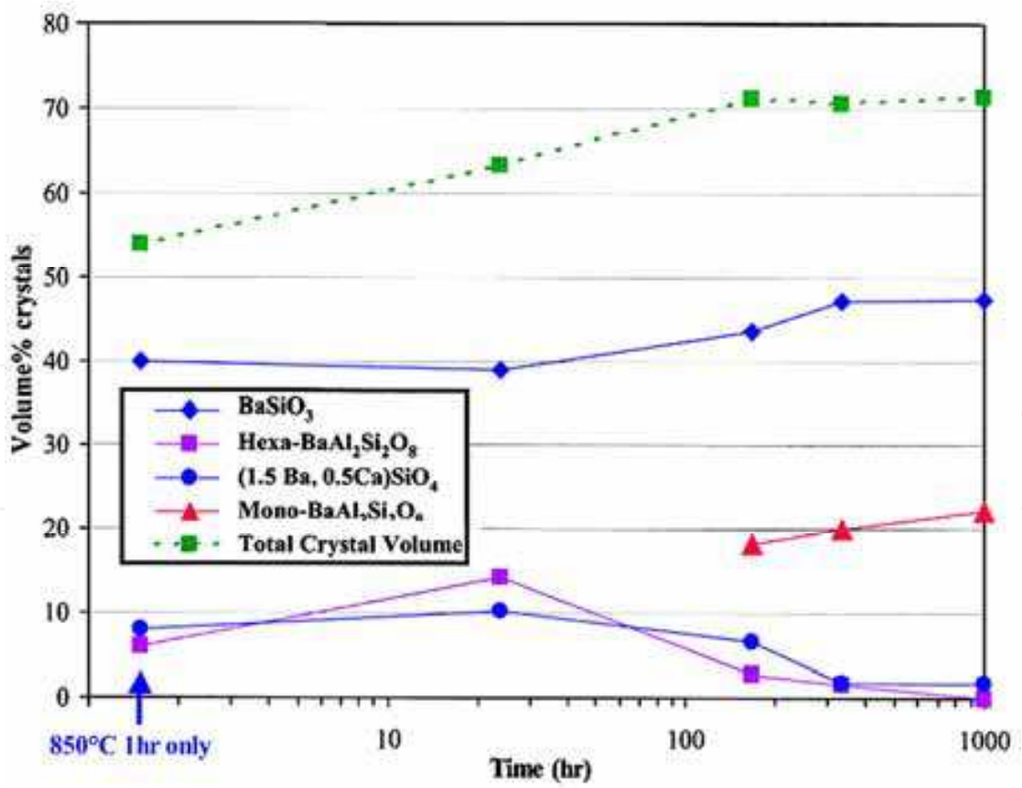

Fig. 1. Quantity of crystalline phase formed in glass-ceramic sealant (G18) as a function of time held in air at 750°C

In general, ceramic crystalline possesses more stable mechanical properties under high temperature than pure amorphous glass. The glass transition temperature of the amorphous glass is about 500°C to 600°C; therefore, the mechanical modulus of the amorphous glass will degrade dramatically over the glass-transition temperature. This causes the pure amorphous glass to overflow during the operation. An aging dependent increase of the volume fraction of the ceramic crystalline in the glass ceramic sealant enhances the mechanical modulus of the sealant at high temperatures to prevent the sealant from overflowing during the operation under stack clamping loads. This will greatly benefit the long-term reliability and performance of SOFCs.

2.2 Evolution of micro-damage of glass-ceramic sealant

During further devitrification of glass under the operating temperatures of SOFCs, not only does the volume fraction of the crystalline phases increase, but also the morphology of the crystalline phases changes. Samples used here for the evolution of micro-damage of glass-ceramic sealant were 3 mm × 4 mm × 45 mm. Ten samples were prepared. They were placed into the furnace and heat treated at 850°C for 1 hour and then aged at 750°C. Five samples were aged for 4 hours, and another five samples were aged for 1,000 hours. To look inside of the glass-ceramic sealant materials, these specimens were cross-sectioned along the central line. The top surface and the cross-section of the specimens were ground to a 600-grit finish and then ultrasonically cleaned with distilled water and acetone like the XRD experiments. Scanning electron microscopy (SEM) was adopted to probe the microstructure of the glass-ceramic sealant material. SEM images of the microstructure of the glass ceramic sealant materials were taken by JEOL JSM-840 with an LaB6 emitter.

Figures 2 and 3 show the typical microstructure of the top and cross-section of the glass ceramic sealant, respectively, after glass paste is spread and is sintered initially. At the end of the initial sintering process, no matter where it is (the surface or the interior of the glass-ceramic sealant), distinct boundaries between the glass (amorphous) phase and the ceramic (crystalline) phase can be observed, and the fibrous and needle-like crystalline structures can be seen clearly in the amorphous glass phase. Some small voids and flaws are also illustrated in the microstructures. The structure of the two phases is relatively intact even with some voids and flaws. The microstructures of the glass ceramic sealant after aging for 1,000 hours at 750°C are depicted in Figures 4 and 5 for the top surface and the cross-section, respectively. Obviously, many more small voids were now present, particularly in the amorphous phase. This occurred not only on the surface, but also the interior of the material. The overall void volume fraction also increased from the volume observed after the initial sintering process shown in Figures 2 and 3. Compared with Figures 2 and 3, the distinct fibrous and needle-like crystals in the amorphous phase disappeared, and smeared/diffused phase boundaries between the glass phase and ceramic phase were observed after aging for 1,000 hours. The CTE of the ceramic phase, in general, was higher than that of the amorphous glass phase (Roos et al., 2007; Brochu et al., 2006; Fei, 1995). The mismatch of the CTE of the ceramic and glass phases will cause different shrinkages of the ceramic phase and glass phase during cooling. The shrinkage of the ceramic phase is much larger than that of the glass phase; therefore, a crack will be created along the weak boundary between the glass phase and the ceramic phase; furthermore, this will possibly create micro-voids, particularly in the glass phase.

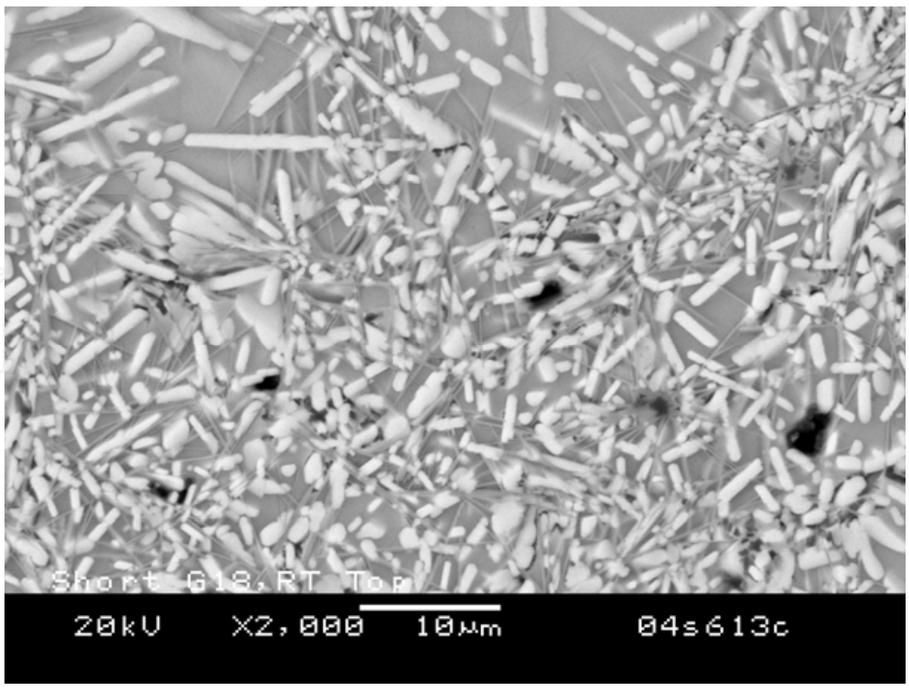

a)

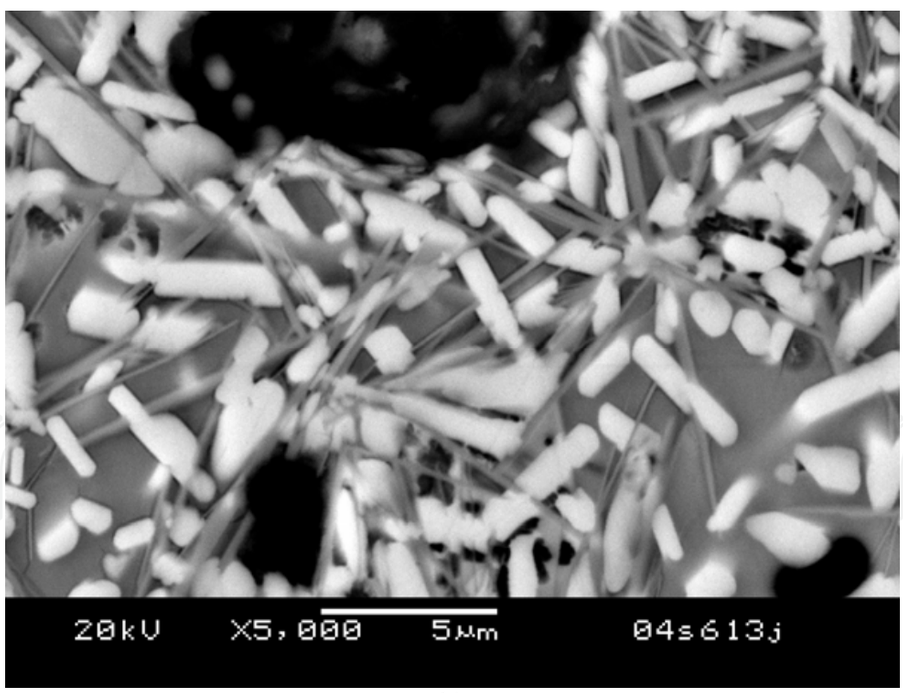

b)

Fig. 2. SEM image of microstructure of top surface of glass-ceramic sealant after initial sintering process: a) magnification: 2000×; b) magnification: 5000×

At room temperature, the glass/ceramic sealant is characterized by brittle material. Small crack and flaw in the brittle materials is dreadful to cause the propagation of the small crack

and flaw under residual tensile stresses induced by the mismatch of CTE of various components, and to lead to failure of the sealant in SOFC.

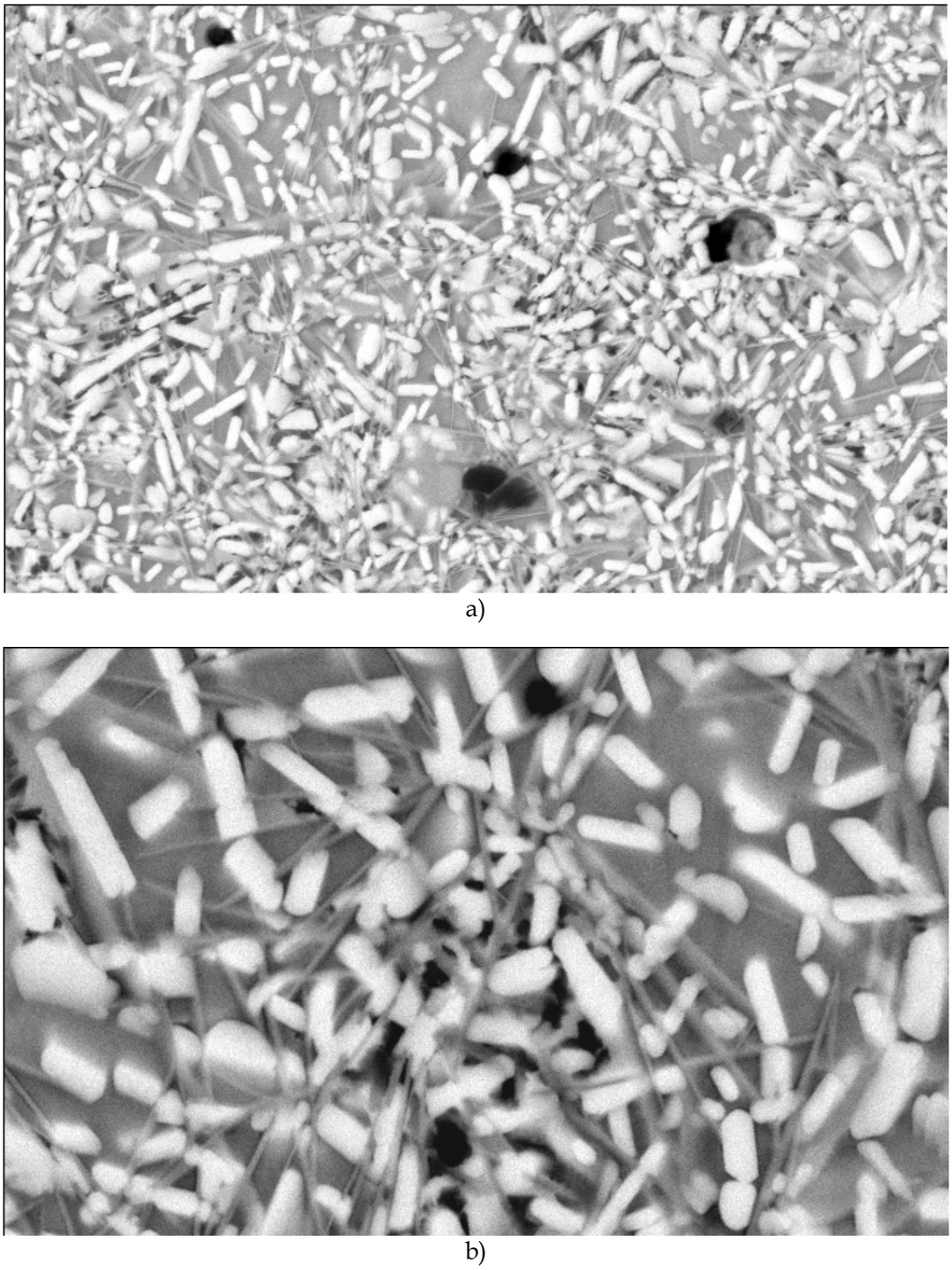

Fig. 3. SEM image of microstructure of cross-section of glass-ceramic sealant after initial sintering process a) magnification: 2000×; b) magnification: 5000×

2.3 Possible self-healing of glass-ceramic sealant

Even though G18 exhibits creep/flow behavior under operating temperatures, its behavior at room temperature can be characterized as being brittle. During thermal cycling, the tensile residual stresses caused by the mismatch of CTEs of various cell components can potentially generate many small cracks and voids in the brittle seal material after cooling down. If left untreated/unhealed, these small cracks in the seal could be detrimental to the overall stack reliability for the next operating cycle.

To gain a deep insight into the behavior of damaged glass ceramic sealant under high temperatures, indentation and four-point bend tests were used on the short crystallized glass ceramic sealant. The short crystallized bend bar was polished to a diamond finish of 3 microns, and its edge was rounded. The polished bend bar was then indented with a Vickers diamond at 2 kg. Five indentations were made within the inner span of the bend bar with the objective to drive the crack under slow crosshead (0.025 mm/min) and stop the crack propagation to observe the damage ahead of the crack tip. As shown in Figure 6, the typical Vickers impressions with perfectly symmetrical, four radial cracks emanating from the four corners were created on the surface of the short crystallized glass ceramic sealant by the Vickers indentation. Under higher magnification for one of the radial cracks (Figure 7), it was observed that crack propagation followed a less tortuous path as compared to typical structural ceramics (Fang et al., 2002; Marliere et al., 2003). The white crystallite in rod shape (likely $BaSiO_3$) appears to be stronger than the featureless glass (gray area) because some crack deflection and bridging were observed as compared to the straight crack path through the gray area (likely the un-crystallized residual glasses). Nevertheless, the glass ceramic sealant used here showed typical brittleness with a single crack at room temperature.

After indentation, the bend bar was placed in a four-point fixture and tested at a slow cross speed of 0.025 mm/min (as compared to the normal speed of 0.5 mm/min) at 750°C. The sample was loaded up to ~20 N and held for a half hour at 750°C , and then was stopped for damage characterization under SEM. It may be seen that all the radial cracks were healed. Figures 8 and 9 show the typical SEM images of the example at low and high magnifications. It is evident that all of the four radial cracks healed completely. One would expect the Vickers impression to tend to smooth (rounding at four sharp corners) slightly during the half hour of soaking at 750°C such that the two radial cracks at N and S directions would be experiencing compressive stress (just like a circular hole) when the bend bar was loaded, and these two radial cracks could heal; however, this was not the case for the other two radial cracks (E and W directions) because they are under tensile stresses upon loading. These experimental observations can serve as evidence that the glass/ceramic sealant material exhibits some degree of self-healing: when reheated again to a high operating temperature, the damage in the glass ceramic sealant may disappear because of the flow of the glass phase, potentially restoring its mechanical property to its undamaged level. Other possible physical explanations for this healing behavior may be the capillary force of the residual glass phase as well as the residual stresses caused by the Vickers indentation.

The advantage of this self-healing behavior of the glass ceramic sealants is that materials with a dramatically different expansion can potentially be used for seals because at the cell operating temperatures, CTE mismatch-induced damage, like micro-voids, can be healed automatically. Then the mechanical performance of the glass ceramic sealant can be restored as undamaged. For SOFC stacks during the operating thermal cycles, the micro-damage in the glass ceramic sealant may be formed when cooling down from the operating

temperature to room temperature. Then the micro-damage may be healed at some threshold temperature.

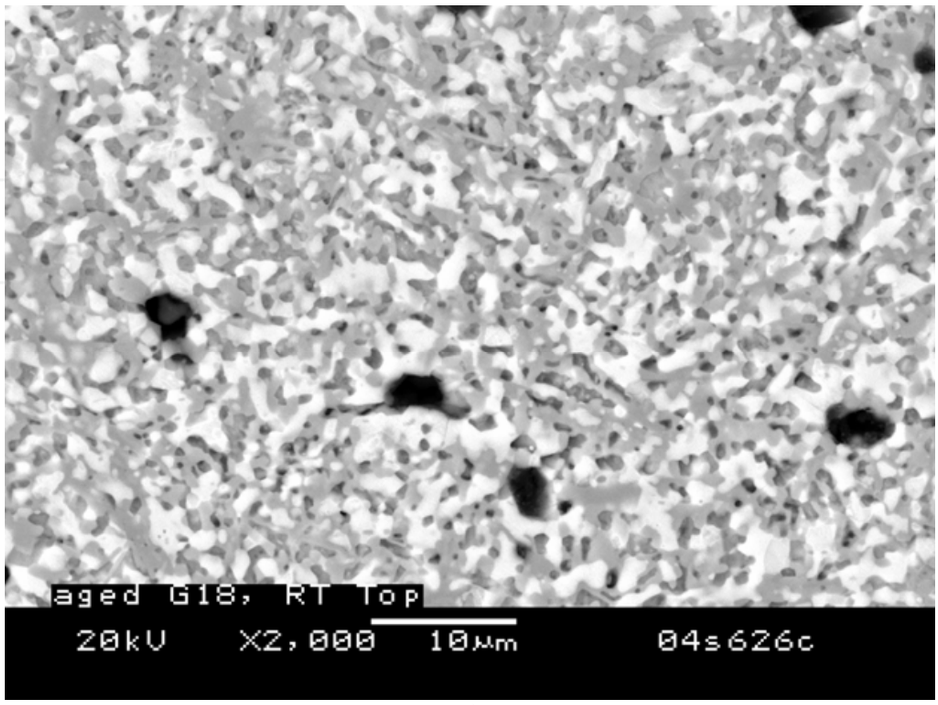

a)

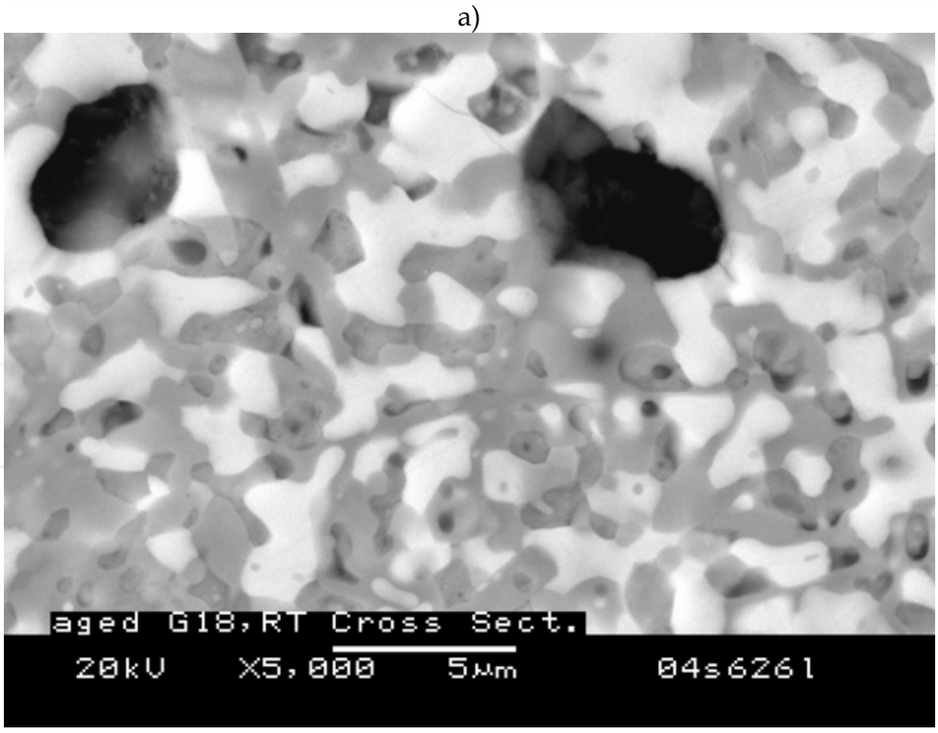

b)

Fig. 4. SEM image of microstructure of top surface of glass-ceramic sealant after 1000 hours of aging at 750°C: a) magnification: 2000×; b) magnification: 5000×

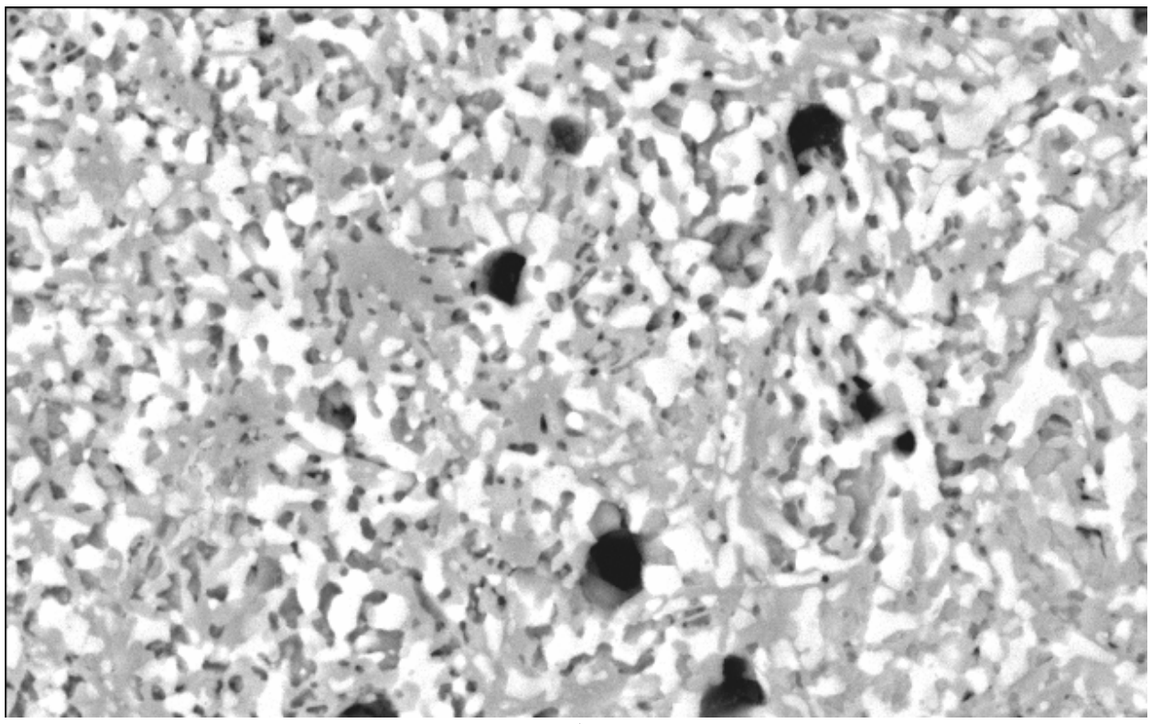

a)

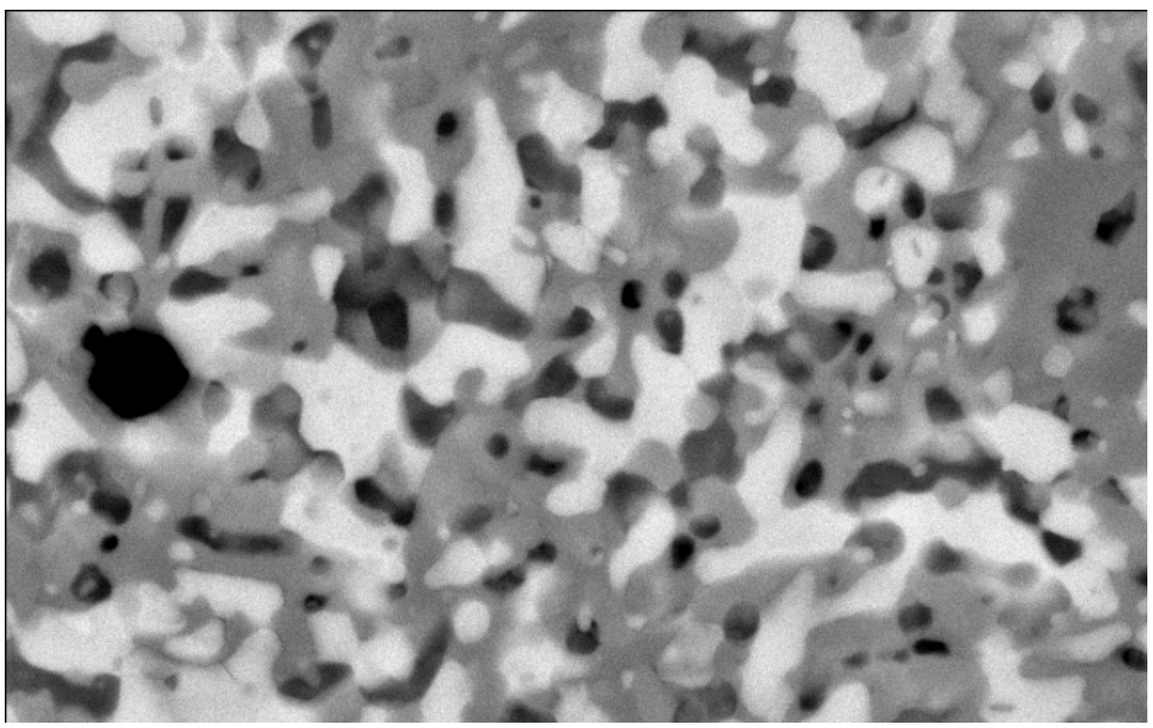

b)

Fig. 5. SEM image of microstructure of cross-section of glass-ceramic sealant after 1000 hours of aging at 750°C: a) magnification: 2000×; b) magnification: 5000×

3. Degradation of mechanical properties of glass-ceramic sealants

The dynamic resonance technique (ASTM C1198) was used to measure the elastic moduli of the specimens of both non-aged and 1000-h aged short crystallized G18 at room and elevated temperatures.[1] The instrument used to measure the resonant frequencies was constructed following ASTM C1198. The specimen was suspended within a resistance-heated furnace using single-crystal, sapphire fibers with beaded ends. Small, narrow notches were cut into the corners of the specimen to accept the fibers. The fibers coupled the specimen to two piezoelectric transducers mounted above the furnace. One transducer was used as a driver, and the other as a receiver. A computer-controlled system was used to send frequency signals sweeping from 20 Hz to 20 kHz through the driver transducer. The signal from the receiving transducer was fed back into the computer, and the resonant frequencies were identified and recorded. Both the transverse and longitudinal resonant frequencies could be reliably detected at the corners of the specimen. Resonant frequency data were then used in calculating the elastic moduli with the following equations (ASTM, 2008):

$$E = 0.9465 \frac{m f_f^2}{b} \frac{L^3}{h^3} T_1 \tag{2}$$

$$G = \frac{4Lmf_t}{bh} \frac{B}{1+A} \tag{3}$$

where E and G are the Young's modulus and shear modulus, respectively; m is the mass of the bar; b, h, and L are the width, thickness, and length of the bar, respectively; f_f represents the fundamental resonant frequency of the bar in flexure; and T_1 denotes the correction factor for the fundamental flexural mode to account for the finite thickness of the bar and Poisson's ratio, etc. The Young's and shear moduli were then used to calculate Poisson's ratio:

$$\mu = (E / 2G) - 1 \tag{4}$$

The precisions of the E, G, and μ values were calculated by propagating the uncertainty of each term through the equations.

The test specimen was a right parallelepiped measuring 50.75 x 25.34 x 5.96 mm. All surfaces were ground smooth. Resonant frequencies were measured at room temperature and in 100°C intervals from 200–800°C. The furnace was heated at a rate of approximately 12°C/min and was held for 15 minutes at each temperature for equilibration.

The measured Young's modulus for the non-aged and 1000-h aged G18 at room and elevated temperature is tabulated in Table 1. Both of the measured Young's modulus and shear modulus for the non-aged and 1000-h aged G18 at room and elevated temperature are shown in Figure 10. For non-aged short crystallized glass/ceramic sealant (G18), both the Young's modulus and shear modulus decrease with an increasing test temperature. The resonant peaks became very broad at about 700°C, making it impossible to differentiate between the longitudinal and transverse peaks with any certainty. This may have been

[1] Shelleman, D. L., & Green, D. J. (2006). *Measurement of Elastic Constants on Sample Supplied by PNNL*, Internal Technical Report, Pacific Northwest National Laboratory, Richland, Washington.

caused by the softening of the glass phase present in these specimens. Additional measurements were taken again at room temperature (30°C) after the high-temperature tests achieved the same moduli as the pre-test values.

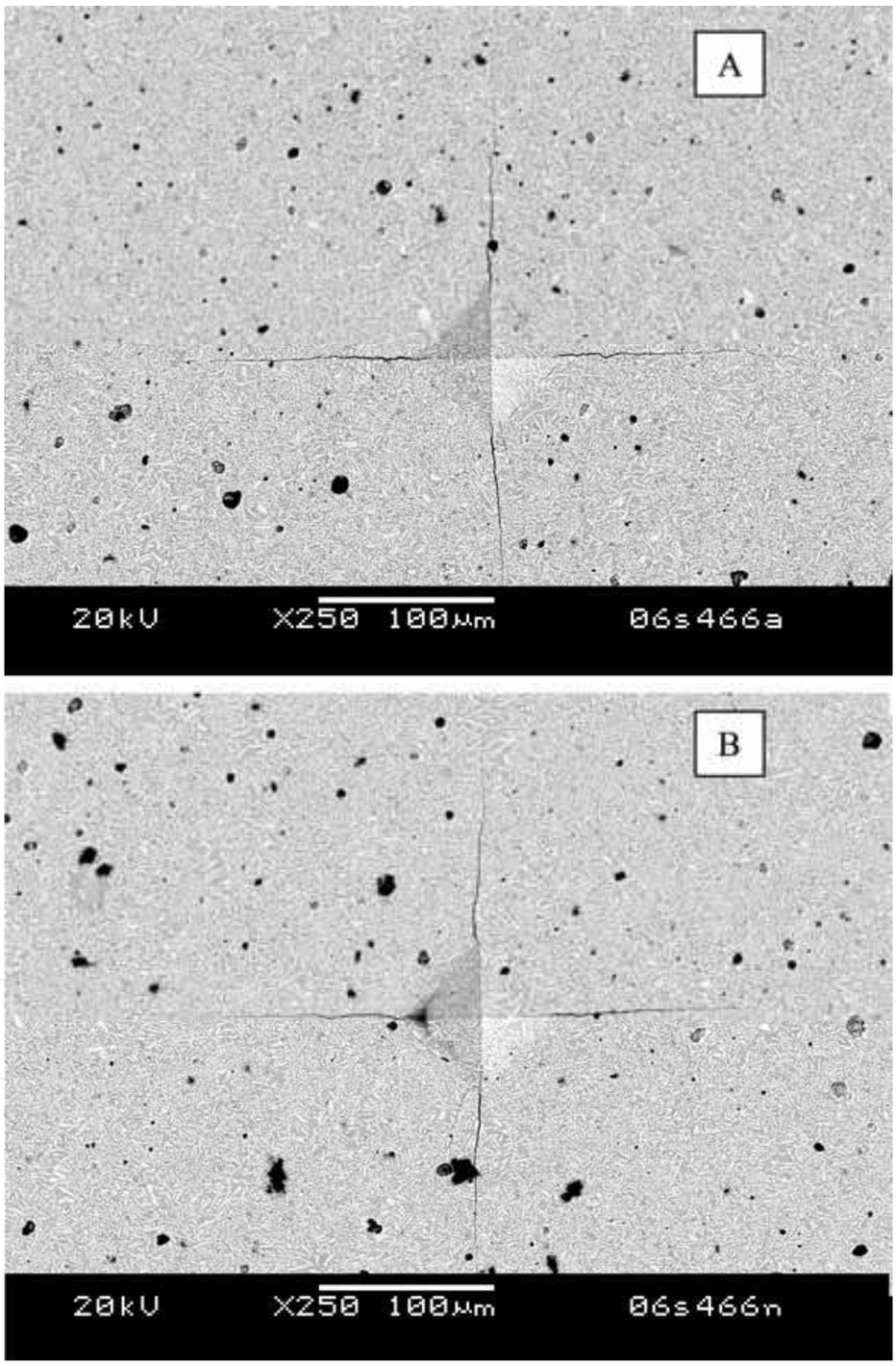

Fig. 6. Typical impression of indentation with Vickers indenter at 2 kg indentation load on polished, short crystallized, glass-ceramic specimen

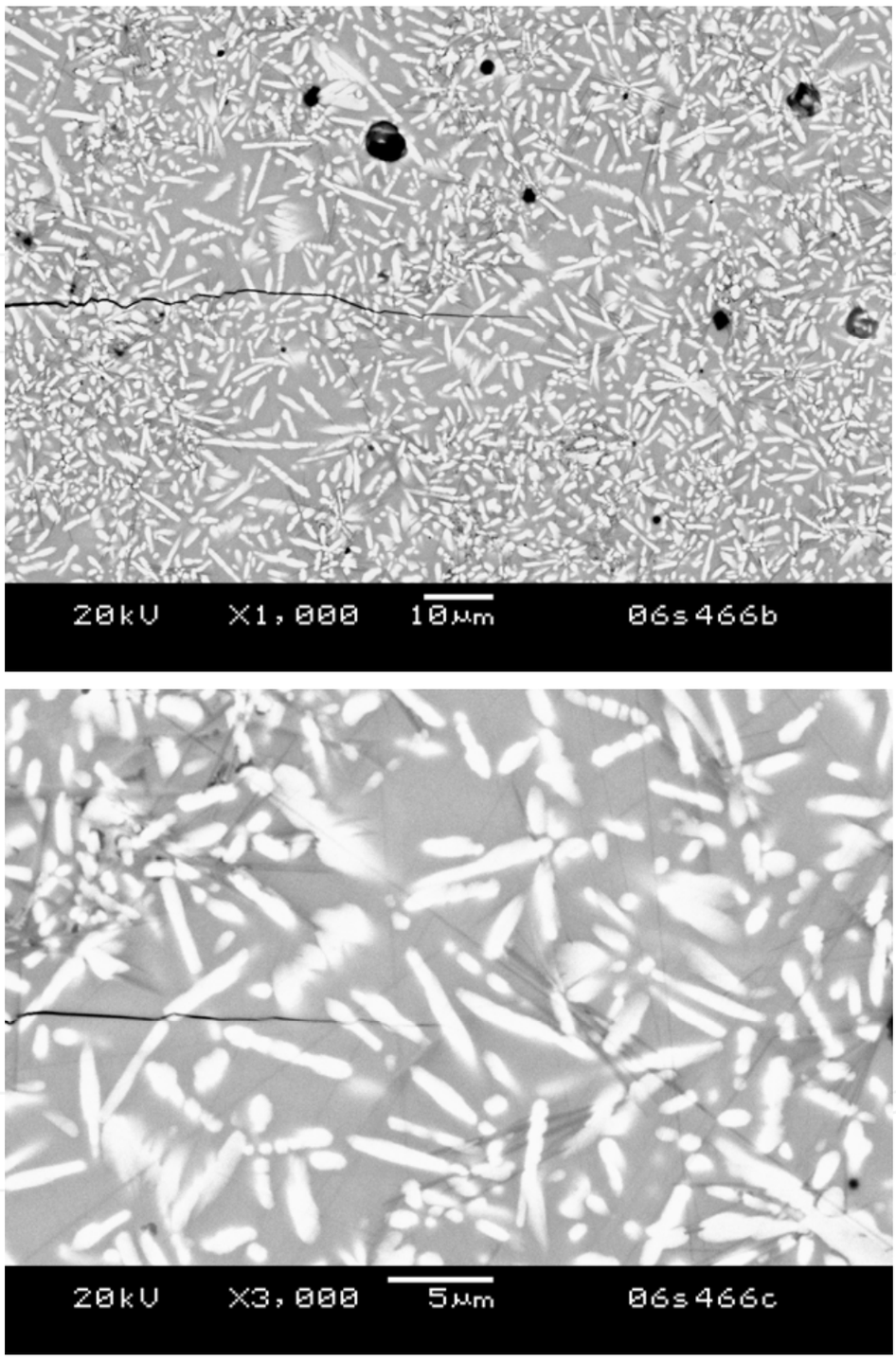

Fig. 7. SEM pictures of indentation impression at the crack tip on polished, short crystallized, glass-ceramic specimen with higher magnification

The measured Young's modulus and shear modulus for the 1000-h aged G18 show some very distinct and interesting features. For temperatures lower than 400°C, both Young's modulus and the shear modulus increase with increasing test temperature. The moduli

exhibit somewhat temperature-independent behaviors from 400°C to 600°C. Above 600°C, the moduli start to decrease with increasing temperature.

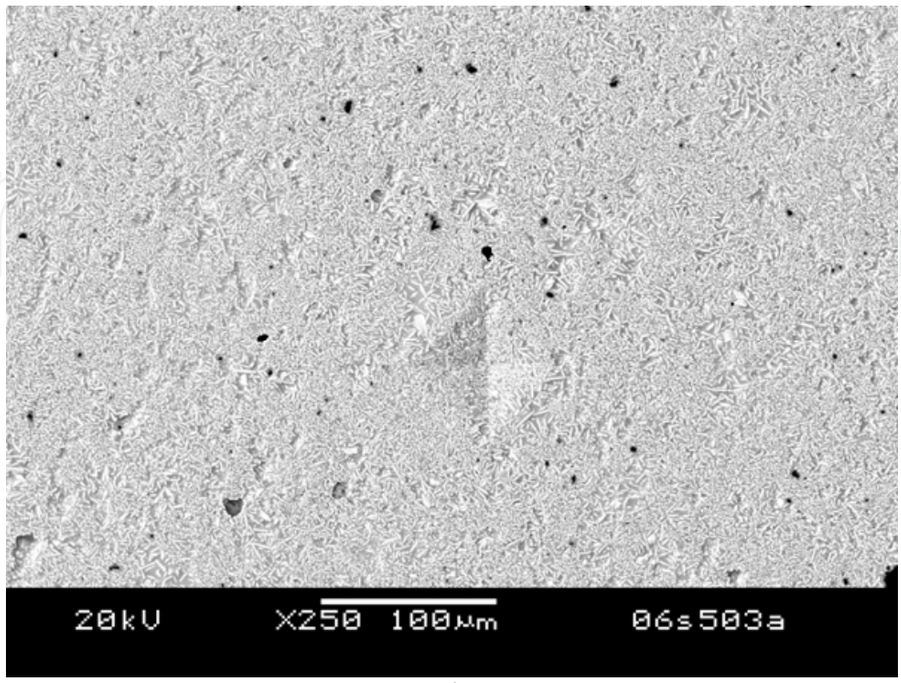

a)

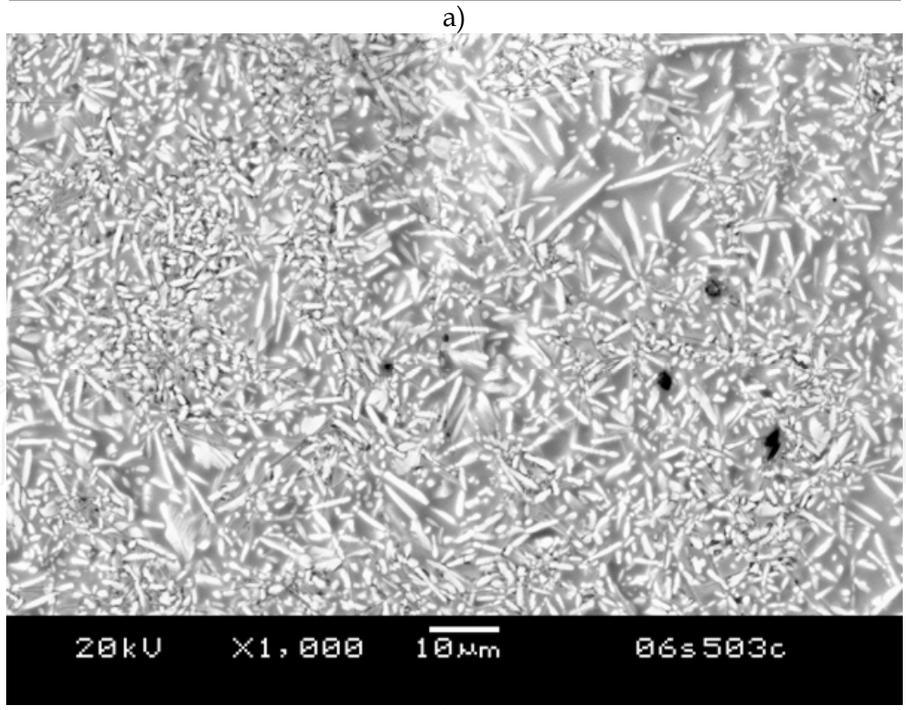

b)

Fig. 8. SEM pictures of the indentation impression on polished, short crystallized, glass-ceramic specimen after it was reheated and loaded to ~20 N at 750°C: a) overview with low magnification, and b) crack tip with high magnification

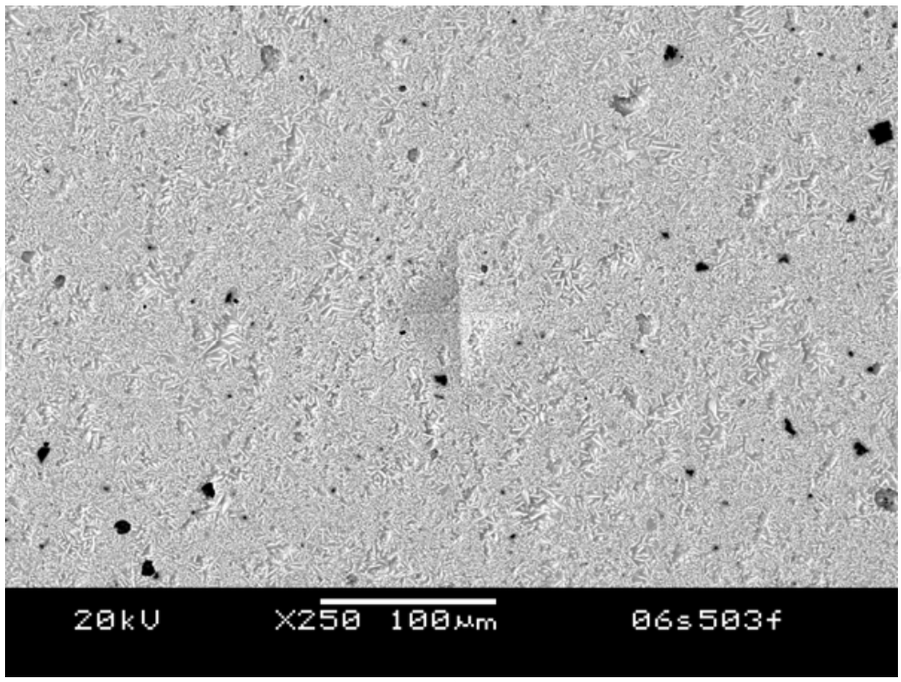

a)

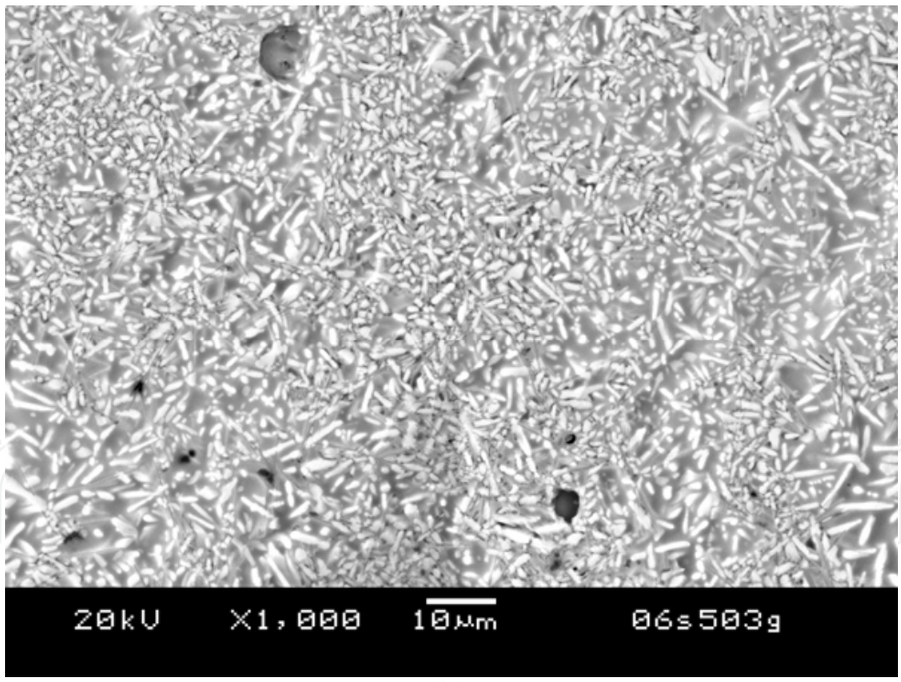

b)

Fig. 9. SEM pictures of the indentation impression on polished, short crystallized, glass-ceramic specimen after it was reheated and loaded to ~20 N at 750°C: a) overview with low magnification, and b) crack tip with high magnification

For temperatures lower than 400°C, the measured modulus for the aged glass ceramic sealant is consistently less than that of the non-aged (short-term aged) glass ceramic. At

about 500°C, the moduli for the aged and non-aged samples cross over. For temperatures above 600°C, the moduli trend reverses itself: the modulus for 1000-h aged G18 is higher than that of the non-aged G18.

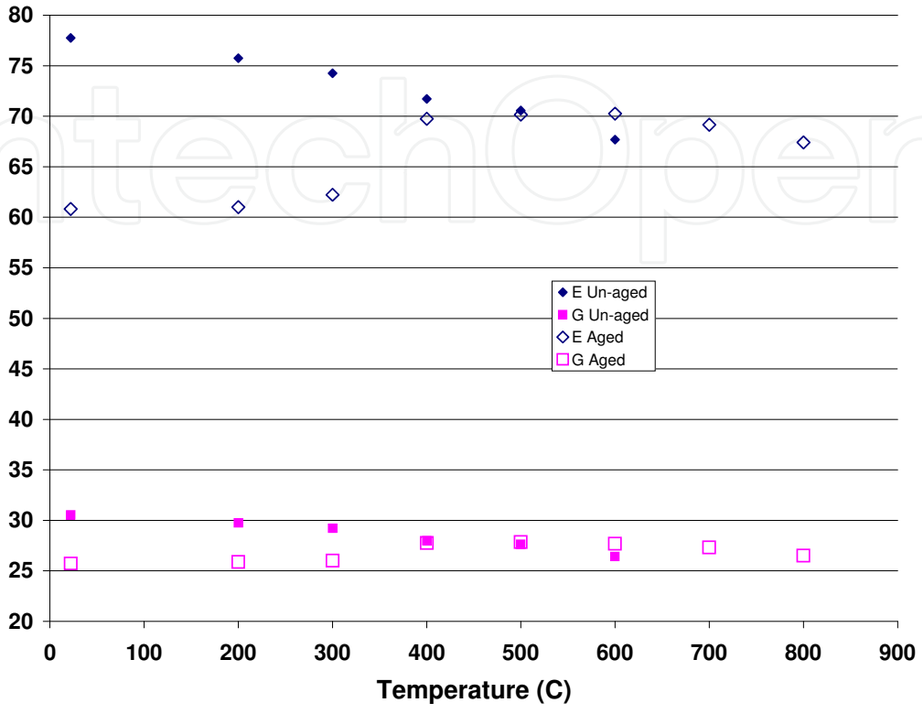

Fig. 10. Young's and shear moduli for aged and un-aged G18 at room and elevated temperatures. The furnace was heated at a rate of approximately 12°C/min, and was held for 15 minutes at each temperature for equilibration

This distinct temperature-dependent modulus behavior for the aged G18 is another motivation for our current work. Our goal is to see whether this unique behavior can be predicted by coupling the various phenomena such as aging, cooling, and reheating-induced self-healing. The eventual goal is to develop a predictive capability for glass ceramic seals such that better seal materials can be developed for improved reliability and durability.

Temperature (°C)	1000-h Aged (GPa)	Un-aged (GPa)
22	60.8 ± 0.3	77.7 ± 0.4
200	61.0 ± 0.3	75.8 ± 0.4
300	62.2 ± 0.3	74.3 ± 0.4
400	69.7 ± 0.3	71.7 ± 0.3
500	70.2 ± 0.3	70.6 ± 0.3
600	70.3 ± 0.3	67.7 ± 0.3
700	69.2 ± 0.3	---------
800	67.4 ± 0.3	---------
30	53.2 ± 0.3	78.1 ± 0.4

Table 1. Young's modulus aged and un-aged G18 at room and elevated temperatures

4. Predicting Young's modulus of glass-ceramic sealant with consideration of aging, micro-damage, and self-healing

4.1 Aging time-dependent volume fraction evolution of crystalline phase

Aging changes the volume fraction of the ceramic phase in the glass ceramic microstructure, hence influencing seal mechanical properties such as Young's modulus, strength, fracture toughness and durability (Han & Tomozawa, 1989; Bhathena et al. 1984; Bentur et al., 1985; Schwarz et al., 2001; Baudin & Villar, 1998). For glass/ceramic sealing materials, the volume fraction of the ceramic crystalline is aging-time dependent under the SOFC operating temperature. At the end of the initial sealing process at 850°C, some volume fraction of the ceramic crystalline is formed. Subjected to the typical operating environment of 750°C, the crystallization process slows down but does not stop. This continuing devitrification causes the volume fraction of the ceramic crystalline in the sealant material to increase with the holding time at the operating temperature.

Assuming that the devitrification of glass/ceramic can reach an asymptotic level after 300 hours of aging/working time at 750°C, the evolution of the volume fraction of the crystalline phases with respect of time t may be expressed as

$$f_C(t) = f_C^{\infty} - (f_C^{\infty} - f_C^0)e^{(-t/A_t)} \tag{5}$$

where f_C^{∞} and f_C^0 represent the volume fractions of the ceramic phase in the stable stage and the initial stage of the sealing process, respectively. A_t represents the characteristic aging time. Note that various crystalline phases are lumped into one term, f_C, in this work.

According to the experimental data shown in Figure 1, the parameters in Eq. (5) can be determined for G18 as:

$$f_C^{\infty} = 72.0, \qquad f_C^0 = 54.0, \qquad A_t = 40.0(hour) \tag{6}$$

These are material-specific parameters that are closely dependent on the glass composition and associated heat treatment processes.

4.2 Aging induced micro-voids in glass-ceramic

Aging at high temperature often leads to material property degradations (Nam & Seferis, 1991; Nam & Seferis 1992). One possible degradation mechanism is the appearance of the voids and cracks (Kim et al., 2002).

To capture the effect of aging and cooling-induced microstructure changes on the mechanical properties of the glass ceramic sealant, a continuum damage mechanics model (Jessen & Plumtree, 1991; Jeong & Adib, 2005; Lemaitre, 2002; Sun et al., in press) is used here as a phenomenological approach to the constitutive modeling of the glass/ceramic seal. The microstructure-level heterogeneous G18 is represented by an equivalent homogeneous material with effective properties. The model accounts for the material damage because of various mechanisms (i.e., void growth, void nucleation and coalescence, decohesion between different phases, etc.) in a phenomenological way through a scalar damage variable, D, that governs the reduction of the homogenized elastic modulus (Sun et al., 2009):

$$E^D(t,T,D) = E(t,T)(1-D) \tag{7}$$

where E^D and E represent the Young's modulus with and without damage, t is time, and T is temperature. D is the quantitative measure of the void volume fraction in comparison with the virgin microstructure.

4.3 Possible self-healing of glass-ceramic seals

It should be mentioned that the concept of self-healing glass seals was first reported by Singh (Singh 2006). The rationale behind this concept is that at the SOFC operating temperature, a sealing glass with appropriate properties can heal cracks created during thermal transients. The advantage of this approach is that materials with dramatically different expansions can potentially be used for seals because at the cell operating temperatures, the CTE mismatch-induced, thermo-mechanical stresses can be relaxed out. If proven feasible, this type of seal can tolerate some of the thermal expansion mismatch and still form a functioning seal between materials with a significant expansion mismatch. However, there are still a number of challenges in making a functioning seal with self-healing glasses. The first challenge is that the glass seal must maintain contact with all the components to be sealed without excess creep/flow at a cell operating temperature of 750°C. Concepts involving various ceramic phase stoppers have been proposed to address this. In addition, the self-healing glass seal must be capable of remaining chemically stable under SOFC operating temperatures for the designed stack operating time.

For SOFC stacks under deep thermal cycles, cracking and micro-voids may occur in the glass ceramic sealant because of the tensile residual stress caused by a CTE mismatch of different components during cooling. However, upon reheating, the damage/crack may be healed at temperatures above some threshold temperature because of the flow behavior of the glass phase. Therefore, the scalar damage D defined in Eq. (7) is temperature and aging-time dependent, which may be simplified as the product of the following uncoupled factors:

$$D = A_D D_T \tag{8}$$

Here A_D is the aging influence function, representing the increase of the micro-void volume fraction with aging time:

$$A_D = 1 - e^{-t/t_c} \tag{9}$$

where t is the aging time, and t_c represents the characteristic time.

D_T in Eq. (8) represents the temperature-dependence of damage, reflecting the possible self-healing behavior of G18 above the threshold temperature, T_{th} :

$$D_T = D_0 \frac{\pi / 2.0 - \arctan[(T - T_{th}) / R]}{\pi} \tag{10}$$

where D_0 is the damage parameter at room temperature, and T_{th} is the threshold temperature above which damage to the glass ceramic composite starts to heal, T is operating temperature and R is a constant.

4.4 Assembly of the phenomenological model

Various formulations and frameworks have been developed to model the mechanical behaviour of composite materials (Bigaud & Hamelin, 1997; Annapragada et al., 2007; Chen

& Argon, 1979; Leble et al., 1999; Ahzi et al., 2003; Makradi et al., 2005). For simplicity, we adopt here the simple Rule of Mixture approach. In general, the Young's modulus of the multi-phase composite materials can be expressed as (Gibson, 2007):

$$E = \sum_{i=1}^{m} f_i E_i \tag{11}$$

where f_i and E_i represent the volume fraction and modulus of the ith phase, and m is the number of the phases in the composite material. The volume fractions of all the phases should satisfy

$$\sum_{i=1}^{m} f_i = 1 \tag{12}$$

In the case of the two phase glass/ceramic sealant composite material, the above equation can be rewritten as

$$E = f_C E_C + (1 - f_C) E_G \tag{13}$$

or

$$E = f_C (E_C - E_G) + E_G \tag{14}$$

where the subscripts "C" and "G" refer to the glass phase and the ceramic phase, respectively. In general, the modulus of the glass phase is temperature dependent, and the modulus of the ceramic crystalline is independent of temperature.
Substituting the aging-time–dependent volume fraction of the ceramic phase, i.e., Eq. (5), into Eq. (14) leads to

$$E(t,T,) = \left(f_C^{\infty} - f_C^0 e^{(-t/A_t)} \right)(E_C - E_G(T)) + E_G(T) \tag{15}$$

Incorporating the effects of micro-damage and self-healing described in Eq. (7–9) into Eq. (15) yields the following phenomenological model describing the elastic modulus of the glass ceramic materials:

$$\begin{aligned} E^D(t,T,D) = & \left[\left(f_C^{\infty} - f_C^0 e^{(-t/A_t)} \right)(E_C - E_G(T)) + E_G(T) \right] * \\ & * \left\{ 1 - \frac{D_0}{\pi}(1 - e^{-t/t_c}) \left[\pi / 2.0 - \arctan\left(\frac{T - T_{th}}{R} \right) \right] \right\} \end{aligned} \tag{16}$$

Again, f_C^{∞} and f_C^0 represent the volume fractions of the ceramic phase in the stable stage and at the initial stage of the sealing process, respectively. A_t represents the characteristic aging time. D_0 is the damage parameter at room temperature, and T_{th} refers to the threshold temperature above which damage to the glass ceramic composite starts to heal. R is a material constant, t is the aging time, and t_c represents the characteristic time for aging-induced micro-damage.

5. Comparison between experimental measurements and predictions

For the phenomenological model described in Eq. (16), the modulus of the ceramic phase is considered to be temperature independent, and the modulus for the glass phase is

considered to be temperature dependent. In general, the Young's modulus of glass drops dramatically over the glass transition temperature, T_g (McGraw, 1952).
The input Young's moduli used for the glass and crystalline phases are shown in Figure 11 in dashed lines (McGraw, 1952). The predicted Young's moduli of G18 under different aging times are shown in solid lines in Figure 11. The following parameters for Eq. (16) are calibrated based on the experimental data:

$$D_0 = 0.24, \quad T_{th} = 375°C, \quad R = 50°C, \quad t_c = 100 \text{ h}$$

With the proposed phenomenological model, reasonably good comparisons between the predicted and measured Young's modulus have been achieved for both the aged and un-aged G18. This is particularly true for temperatures lower than 600°C. Above 600°C, the predicted modulus decreases more rapidly with temperature than the measured data. This is because the predicted modulus is very sensitive to the input temperature-dependent modulus for the glass phase. For temperatures above 600°C, the Young's modulus for glass may vary dramatically (Bourhis et al., 2001; Andrews, 1924). The exact high-temperature Young's modulus for regular glass is rarely reported, and the high-temperature Young's modulus for the glass phase in G18 has not yet been separately determined. Therefore, for temperatures above 600°C, the glass moduli used in Figure 10 could have been much lower than the actual values.
It is interesting to note that, by considering the combined effects of aging, micro-voids, and self-healing, the distinct feature of the moduli "cross-over" can be predicted by the the following simple phenomenological model: below 500°C, the 1000-h aged sample has a lower Young's modulus compared to the 4-h aged sample; above 500°C, the trend reverses itself when considering self-healing of the glassy phase.

6. Conclusions

We have investigated experimentally the effects of aging time, micro-damage induced by cooling down from the operating temperature to room temperature, and self-healing when reheating to operating temperatures on the microstructure and mechanical properties of a glass ceramic sealant. This sealant, a glass ceramic material for SOFC sealing applications, was developed at PNNL. The combined effects of aging, cooling-induced micro-voids, and possible reheating-related self-healing were examined and modeled with some simple, phenomenological models. After the initial sealing process, the crystallization process of G18 slows down but does not stop, and the volume fraction of the crystalline phase increases with aging/working time. In addition, aging causes the diffusion/smearing of the boundaries between the crystalline and the amorphous phases and potentially changes the mechanical properties of the amorphous phase.
Upon cooling to room temperature, shrinkage micro-voids form because of the CTE differences between the crystalline and the amorphous phases. On the stack level, cooling-induced micro-cracks are also likely to occur because of the CTE mismatch between different stack components. These micro-voids and micro-cracks can noticeably degrade the Young's modulus of the glass ceramic seal at room temperature. However, when reheated back to SOFC working temperatures, this study shows that G18 does exhibit some degree of self-healing behaviors because of the flow characteristics of the glass phase at high temperatures. Therefore, the mechanical properties, i.e., the Young's modulus of the glass/ceramic seal material, can be potentially restored to an undamaged level at high temperatures.

The phenomenological model based on some simple mechanical analogs has been developed to capture the above-described mechanical behaviors of glass ceramic seal materials. The aging-time–dependent, crystalline phase evolution model was first developed to describe the increase of crystalline content due to the continuing devitrification during operation. A continuum damage mechanics model was adapted to model the effects of micro-voids and self-healing. Reasonably good comparisons between the measured and the predicted temperature-dependent Young's modulus have been obtained. The modeling parameters presented here were calibrated with the experimental data for G18, and yet the modeling framework should be applicable to glass/ceramic seals in general. The model can be further developed to account for the effects of various processing parameters on the mechanical properties of glass/ceramic seal materials.

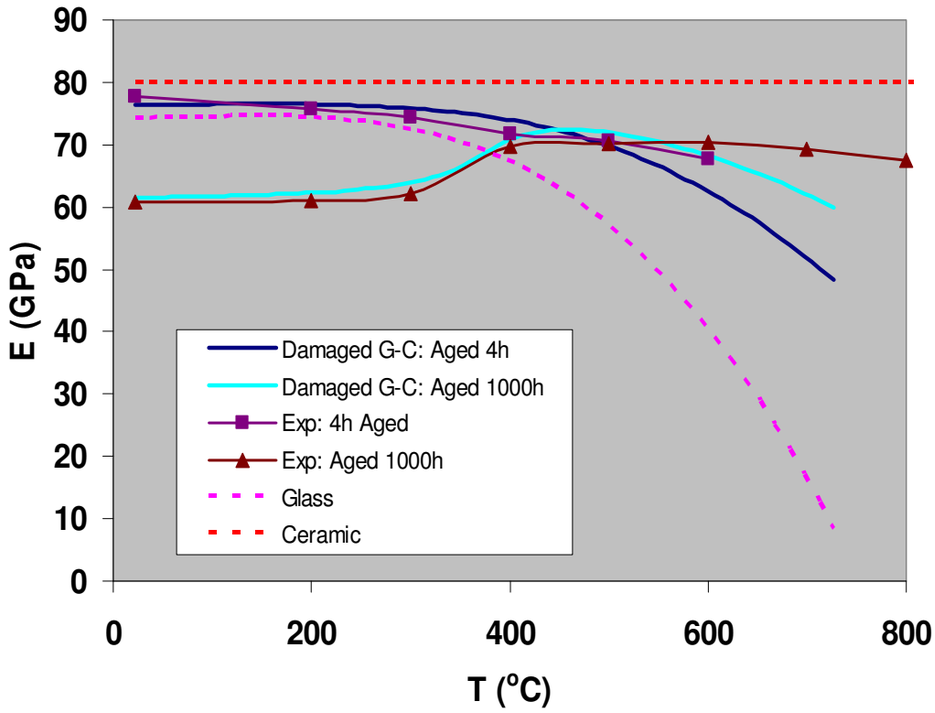

Fig. 11. Predicted and measured Young's modulus versus temperature

7. Acknowledgments

Pacific Northwest National Laboratory is operated by Battelle for the U.S. Department of Energy under Contract DE-AC05-76RL01830. The work was funded as part of the Solid-State Energy Conversion Alliance Core Technology Program by the U.S. Department of Energy's National Energy Technology Laboratory.

8. References

Ahzi, S., Makradi, A., Gregory, R., & Edie, D. (2003). Modeling of deformation behavior and strain-induced crystallization in poly(ethylene terephthalate) above the glass transition temperature. *Mechanics of Materials,* Vol. 35, pp. 1139–1148.

Andrews, J. P. (1924). The Variation of Young's Modulus at High Temperatures. *Proc. Phys. Soc.*, Vol. 36, pp. 169–177.

Annapragada, S. R., Sun, D., & Garimella, S. V. (2007). Prediction of Effective Thermo-Mechanical Properties of Particulate Composites. *Computational Materials Science*, Vol. 40, No. 2, pp. 255–266.

ASTM. (2008). Standard Test Method for Dynamic Young's Modulus, Shear Modulus, and Poisson's Ratio for Advanced Ceramics by Sonic Resonance, ASTM, C1198, *American Society for Testing and Materials*.

Azároff, L. V., Kaplow, R., Kato, N., Weiss, R. J., Wilson, A. J. C., & Young, R. A. (1974). *X-Ray Diffraction*. McGraw-Hill, Columbus, Ohio.

Baudin, C., & Villar, M. P. (1998). Structural and Morphological Transformations of the (NH_4, Na)-exchanged Zeolites 4A, 13X and Synthetic Mordenite by Thermal Treatment. *Journal of the American Ceramic Society,* Vol. 81, No. 10, pp. 2741–45.

Bentur, A., Ben-Bassat, M., Schneider, D. (1985). Durability of glass fibre reinforced cerents with different alkali resistant fibres. *Journal of the American Ceramic Society*, Vol. 68, No. 4, pp. 203–208.

Bhathena, N., Hoagland, R. G., & Meyrick, G. (1984). Effects of Particle Distribution on Transformation-Induced Toughening in an MgO-PSZ. *Journal of the American Ceramic Society*, Vol. 67, No. 12, pp. 799–805.

Bigaud, D., & Hamelin, P. (1997). Mechanical properties prediction of textile-reinforced composite materials using a multiscale energetic approach. *Composite Structures*, Vol. 38, No. 1-4, pp. 361–71.

Bourhis, E. L., Gadaud, P., Guin, J. P., Tournerie, N., Zhang, X. H., Lucas, J., & Rouxel, T. (2001). Temperature dependence of the mechanical behaviour of a GeAsSe glass. *Scripta Materilia,* Vol. 45, pp. 317–323.

Brochu, M., Gauntt, B. D., Shah, R., Miyake, G., & Loehman, R. E. (2006. Comparison between barium and strontium-glass composites for sealing SOFCs. *Journal of the European Ceramic Society*, Vol. 26, No. 15, pp. 3307–3313.

Chen, I. W., & Argon, A. S. (1979). Steady-State Power-Law Creep in Heterogeneous Alloys with Coarse Microstructures. *Acta Metallurgica*, Vol. 27, pp. 785–791.

Choi, S. R., & Bansal, N. P. (2005). Mechanical properties of SOFC seal glass composites. *Mechanical, Ceramic Engineering and Science Proceedings*, Vol. 26, No.4, pp. 275–283.

Chou, Y. S., Stevenson, J. W., & Chick, L. A. (2003). Novel compressive mica seals with metallic interlayers for solid oxide fuel cell applications. *Journal of the American Ceramic Society*, Vol. 86, No. 6, pp. 1003–1007.

Chung, B. W., Chervin, C. N., Haslam, J. J., Pham, A., Glass, R. S. (2005). Development and characterization of a high performance thin-film planar SOFC stack. *Journal of the Electrochemical Society*, Vol. 152, No. 2, pp. A265–A269.

Fang, Y., Ravi-Chandar, K., & White, K. W. (2002). Influence of surface residual stress state on crack path evolution in polycrystalline alumina. *Journal of the American Ceramic Society*, Vol. 85, No. 7, pp. 1783–87.

Fei, Y. (1995). *Mineral Physics and Crystallography, A Handbook of Physical Constants*, AGU Reference Shelf 2, the American Geophysical Union, Washington, D.C.

Fergus, J. W. (2005). Sealants for solid oxide fuel cells. *Journal of Power Sources*, Vol. 147, pp. 46–47.

Gibson, R. F. (2007). *Principles of Composite Material Mechanics*, pp. 91–101, CRC Press, Boca Raton, Florida.

Han, W. T., & Tomozawa, M. (1989). Mechanism of mechanical strength increase of soda-lime glass by aging. *Journal of American Ceramic Society*, Vol. 72, No. 10, pp. 1837–1843.

Jeong, J., Adib, H., & Pluvinage, V. (2005). Proposal of new damage model for thermal shock based on dynamic fracture on the brittle materials. *Journal of Non-Crystalline Solids*, Vol. 351, No. 24–26, pp. 2065–75

Jessen, S. M., & Plumtree, A. (1991). Continuum damage mechanics applied to cyclic behaviour of a glass fibre composite pultrusion. *Composites*, Vol. 22, No. 3, pp. 181–190.

Kim, J., Lee, W., Tsai, S. W. (2002). Modeling of mechanical property degradation by short-term aging at high temperatures. *Composites: Part B*, Vol. 33, pp. 531–543.

Lahl, N., Singheiser, L., Hilpert, K., Singh, K., & Bahadur, D. (1999). In: Aluminosilicate glass ceramics as sealant in SOFC stacks, pp. 1057-65, *Proceedings of the Sixth International Symposium on Solid Oxide Fuel Cells*, The Electrochemical Society, Pennington, New Jersey, 1999.

Leble, P., Dong, M., & Schmauder, S. (1999). Self-consistent matricity model to simulate the mechanical behavior of interpenetrating microstructures. *Computational Materials Science*, Vol. 15, pp. 455–465.

Lemaitre, J. (2002). Introduction to Continuum Damage Mechanics. In: *Continuum Damage Mechanics of Materials and Structures*, Edited by O. Allix, &F. Hild, pp. 235–238, Elsevier Science Ltd, Amsterdam.

Makradi, A., Ahzi, S., Gregory, R. V. & Edie, D. D. (2005). A two-phase self-consistent model for the deformation and phase transformation behavior of polymers above the glass transition temperature: Application to PET. *International Journal of Plasticity*, Vol. 21, No. 4, pp. 741–758.

Marliere, C., Despetis, F., & Phalippou, J. (2003). Crack path instabilities in DCDC experiments in the low speed regime. *Journal of Non-Crystalline Solids*, Vol. 316, No. 1, pp. 21–27.

McGraw, D. A. (1952). Method for determining Young's modulus of glass at elevated temperatures. *Journal of the American Ceramic Society*, Vol. 35, No. 1, pp. 22–27.

Meinhardt, K. D., Vienna, J. D., Armstrong, T. R., & Pederson, L. R. (2002). Glass-Ceramic Material and Method of Making. U. S. Patent 6 430 966.

Nam, J., & Seferis, J. C. (1992). Generalized composite degradation kinetics for polymeric systems under isothermal and nonisothermal conditions. *Journal of Polymer Science, Part B: Polymer Physics*, Vol. 30, pp. 455–63.

Nam, J., Seferis, J. C. (1991). A composite methodology for multistage degradation of polymers. *Journal of Polymer Science, Part B: Polymer Physics*, Vol. 29, pp. 601–608.

Nielsen, K. A., Solvang, M., Nielsen, S. B. L., Dinesen, A. R., Beeaff, D., Larsen, P. H. (2007). Glass composite seals for SOFC application. *Journal of the European Ceramic Society*, Vol. 27, No. 2–3, pp. 1817–22.

Roos, C., Becker, O., & Siebers, F. (2007). Microstructure and stresses in a keatite solid-solution glass-ceramic. *Journal of Materials Science*, Vol. 42. pp. 50–58.

Schwarz, I., Stranz, M., Bonnet, & M., Petermann, J. (2001). Changes of mechanical properties in cold-crystallized syndiotactic polypropylene during aging. *Collid Polymer Science*, Vol. 279, pp. 506–512.

Simner, S. P., & Stevenson, J. W. (2001). Compressive mica seals for SOFC applications. *Journal of Power Sources*, Vol. 102, pp. 310–316.

Singh, R. N. (2007). Sealing Technology for Solid Oxide Fuel Cells (SOFC). *International Journal of Applied Ceramic Technology*, Vol. 4, No. 2, pp. 134–144.

Singh, R. N. (2006). High-Temperature Seals for Solid Oxide Fuel Cells (SOFC). *Journal of Materials Engineering and Performance*, Vol. 15, No. 4, pp. 422–426.

Smeacetto, F., Salvo, M., Ferraris, M., Cho, J., Boccaccini, A. R. (2008). Glass-ceramic seal to join Crofer 22 APU alloy to YSZ ceramic in planar SOFCs. *Journal of the European Ceramic Society*, Vol. 28, No. 1, pp. 61–68.

Sun, X., Liu, W. N., Chen, W. N., & Templeton, D. (2009). Modeling and Characterization of Dynamic Failure of Soda-lime Glass Under High Speed Impact. *Journal of Impact Engineering*, Vol. 36, No. 2, pp. 226-234.

Teagan, W. P., Thijssen, J. H. J. S., Carlson, E. J., & Read, C. J. (2000). Current and Future Cost Structures of Fuel Cell Technology Alternatives. In: *Procedures of the 4th European Solid Oxide Fuel Cell Forum*, A. J. McEvoy (Ed.), Lucerne, Switzerland, Vol. 2, pp. 969–980.

Weil, K. S., Deibler, J. E., Hardy, J. S., Kim, D. S., Xia, G. G., Chick, L. A., & Coyle, C. A. (2004). Rupture testing as a tool for developing planar solid oxide fuel cell seals. *Journal of Materials Engineering and Performance*, Vol. 13, No. 3, pp. 316–326.

Yang, Z., Meinhardt, K. D., Stevenson, J. F. (2003). Chemical compatibility of barium-calcium-aluminosilicate-based sealing glasses with the ferritic stainless steel interconnect in SOFCs. *Journal of the Electrochemical Society*, Vol. 150, No. 8, A1095–A1101.

Yang, Z., Xia, G., Meinhardt, K. D., Weil, K. S., & Stevenson, J. W. (2004). Chemical stability of glass seal interfaces in intermediate temperature solid oxide fuel cells. *Journal of Materials Engineering and Performance*, Vol. 13, No. 3, pp. 327–334.

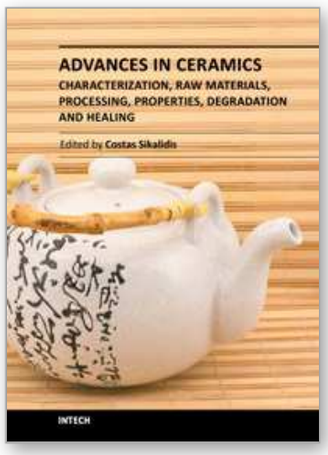

Advances in Ceramics - Characterization, Raw Materials, Processing, Properties, Degradation and Healing

Edited by Prof. Costas Sikalidis

ISBN 978-953-307-504-4
Hard cover, 370 pages
Publisher InTech
Published online 01, August, 2011
Published in print edition August, 2011

The current book consists of eighteen chapters divided into three sections. Section I includes nine topics in characterization techniques and evaluation of advanced ceramics dealing with newly developed photothermal, ultrasonic and ion spattering techniques, the neutron irradiation and the properties of ceramics, the existence of a polytypic multi-structured boron carbide, the oxygen isotope exchange between gases and nanoscale oxides and the evaluation of perovskite structures ceramics for sensors and ultrasonic applications. Section II includes six topics in raw materials, processes and mechanical and other properties of conventional and advanced ceramic materials, dealing with the evaluation of local raw materials and various types and forms of wastes for ceramics production, the effect of production parameters on ceramic properties, the evaluation of dental ceramics through application parameters and the reinforcement of ceramics by fibers. Section III, includes three topics in degradation, aging and healing of ceramic materials, dealing with the effect of granite waste addition on artificial and natural degradation bricks, the effect of aging, micro-voids, and self-healing on mechanical properties of glass ceramics and the crack-healing ability of structural ceramics.

INTECH
open science | open minds

InTech Europe
University Campus STeP Ri
Slavka Krautzeka 83/A
51000 Rijeka, Croatia
Phone: +385 (51) 770 447
Fax: +385 (51) 686 166
www.intechopen.com

InTech China
Unit 405, Office Block, Hotel Equatorial Shanghai
No.65, Yan An Road (West), Shanghai, 200040, China
中国上海市延安西路65号上海国际贵都大饭店办公楼405单元
Phone: +86-21-62489820
Fax: +86-21-62489821

IntechOpen